Journal of Porous Media 8(1), 13–29 (2005)

Numerical Solution of Turbulent Channel Flow Past a Backward-Facing Step with a Porous Insert Using Linear and Nonlinear k–ε Models

Marcelo Assato,[1] Marcos H. J. Pedras,[2] and Marcelo J. S. de Lemos[1]*

[1]Departamento de Energia—IEME, Instituto Tecnológico de Aeronáutica—ITA, 12228-900-São José dos Campos—SP, Brazil
*E-mail: delemos@mec.ita.br
[2]Instituto de Pesquisa e Desenvolvimento—IP&D, Universidade do Vale do Paraiba—UNIVAP, 12244-000—São José dos Campos—SP, Brazil

ABSTRACT

This work presents a numerical investigation of turbulent flow past a backward-facing-step channel with a porous insert using linear and nonlinear eddy viscosity macroscopic models. The nonlinear turbulence models are known to perform better than classical eddy-diffusivity models due to their ability to simulate important characteristics of the flow. Turbulence-driven secondary motion and the effects of streamline curvature on turbulence cannot be fully accounted for with simpler isotropic models. Parameters such as porosity, permeability, and thickness of the porous insert are varied in order to analyze their effects on the flow pattern, particularly on the damping of the recirculating bubble after the porous insertion. The numerical technique employed for discretizing the governing equations is the control-volume method. The SIMPLE algorithm is used to correct the pressure field. The classical wall function is utilized in order to handle flow calculation near the wall. Comparisons of results simulated with both linear and nonlinear turbulence models are shown.

Received August 17, 2002; Accepted July 24, 2003

NOMENCLATURE

a	porous insert thickness (m)	$\bar{\mathbf{u}}_D$	average surface velocity (m/s)
c_F	Forchheimer coefficient	U_i	fluid inlet velocity (m/s)
c_{1NL}, c_{2NL}, c_{3NL}	coefficients of nonlinear model	$U_{D\parallel}$	average surface velocity component parallel to the interface (m/s)
c_μ, $c_{1\varepsilon}$, $c_{2\varepsilon}$	turbulence model constants	x_R	reattachment length (m)
c_k	constant for macroscopic turbulence model	**Greek symbols**	
H	step height (m)	β	interface stress jump coefficient
K	porous media permeability (m^2)	ϕ	porosity
L	recirculation length (m)	μ	fluid molecular viscosity ($Ns/m^{2)}$
n	coordinate normal to the interface (m)	ρ	fluid density (kg/m^3)
$\langle\bar{p}\rangle$	intrinsic average pressure (N/m^2)	σ_k, σ_ε	turbulence model constants

INTRODUCTION

Turbulent recirculating bubbles appear in many flows of practical interest and are usually related to mechanical energy losses within the fluid. Flows past a backward-facing step, over sinusoidal surfaces or inside diffusers are examples of such configurations. Sometimes attenuation or even suppression of the recirculating bubble is desirable. Inserts such as honeycombs, screens, or other devices to redistribute the flow are frequently applied in wind tunnels where a uniform flow with low turbulence intensity is required at the test section. Depending on certain parameters, such as insert type, thickness, porosity, and directional permeability, such components may be treated as a porous medium positioned within the flow. For simulating turbulence within permeable media, several macroscopic models have been developed (de Lemos & Pedras, 2001; Lage et al., 2002), some of which based on the so-called "double decomposition" concept. Such an idea has been applied to simulate flow (Pedras & de Lemos, 2000, 2001a–c, 2003), non-buoyant heat transfer (Rocamora & de Lemos, 2000a), buoyancy effects (de Lemos & Braga, 2003, Braga & de Lemos, 2004), mass transfer (de Lemos & Mesquita, 2003) and double-diffusive convection (de Lemos & Tofaneli, 2004) in porous media. In addition, many engineering problems have flows involving interfaces between a porous medium and a clear domain. The problem of boundary conditions at the porous medium–clear fluid interface has been dealt by several authors (Beavers and Joseph, 1967; Vafai and Tien, 1981; Vafai and Kim, 1990; Ochoa Tapia and Whitaker, 1995). Recently, analytical (Kuznetsov, 1996, 1997, 1999) and numerical (Silva and de Lemos, 2003a) solutions for laminar flow in composite channels have been considered, in addition to simulation of turbulent flows in such systems (Silva and de Lemos, 2003b).

More specifically, the problem of flow over a porous block in a channel and past a backward-facing step with porous inserts has been studied by Rocamora and de Lemos (2000b,c) and by Chan et. al. (2000). Both works presented laminar and turbulent results with forced convective heat transfer. They used, for modeling turbulent flow, a two-equation linear k–ε-model with wall function for both the fluid region and the porous medium. Rocamora and de Lemos (2000b,c) treat the interface between the porous medium and the clear fluid following the work by Ochoa Tapia and Whitaker (1995). Chan et. al. (2000) considered the flow at the interface between the fluid and porous medium as being continuous. The presence of the Brinkman's extension model (Brinkman, 1948) in the porous media equation eliminates the need for imposing an explicit interface condition, in accordance with Nield and Bejan (1999).

In this work, numerical results for turbulent flow past a backward-facing step in a channel with a porous insert are presented. Both *linear* and *nonlinear* eddy viscosity macroscopic models are employed. Here, the boundary conditions at the porous medium–clear fluid interface are the same as those used by Rocamora and de Lemos (2000b,c).

Accordingly, it is well established in the literature that clear fluid linear eddy-viscosity turbulence models (LEVM) do not, on the whole, cope well with strong streamline curvature arising, for example, in flows over curved surfaces. And yet, turbulence-driven secondary motion and directional effects due to buoyancy cannot, due to absence of information on individual stresses, be fully simulated with LEVM. In spite of that, they are often used for engineering computations due to the numerical robustness obtained via their linear *stress-strain rate* relationship (Jones and Launder, 1972). This diffusion-like approach makes the numerical solution stable, with the model easily adaptable to existing computer code architectures. The nonlinear eddy-viscosity models (NLEVM), which represent an extension of the LEVM, have shown good performance in flows where the Reynolds normal stresses play an important role (Assato and de Lemos, 2000, 2001) in correcting the deficiencies presented by the LEVM. They basically follow the procedures used in obtaining constitutive equations for laminar flow of non-Newtonian fluids (Rivlin, 1957). An example is the work of Speziale (1987). Essentially, the observed relationship between laminar flow of viscoelastic fluids and turbulent flow of Newtonian substances has motivated developments of such NLEVM (Lumley, 1970). The basic advantage of the NLEVM over other more complex models, e.g., the algebraic stress models (ASM) (Rodi, 1972; de Lemos and Sesonske, 1985; de Lemos, 1988), lies in the achieved computational savings (roughly 25–50% less computing time).

Therefore, in this article comparisons of results simulated with both linear and nonlinear k–ε turbulence models for turbulent flow through a backward-facing-step channel are shown. Some important parameters such as porosity, permeability, and thickness of the porous insert are varied and their effects on the flow are assessed.

MACROSCOPIC TRANSPORT AND CONSTITUTIVE EQUATIONS

The development presented in (Pedras and de Lemos, 2001a–c, 2003) assumes single-phase flow in a saturated, rigid porous medium (ΔV_f independent of time), for which a time-averaged operation on a variable commutes with a space average. For this situation Pedras and de Lemos (2001a) present the following macroscopic equations system.

Macroscopic Continuity Equation

$$\nabla \cdot \bar{\mathbf{u}}_D = 0 \tag{1}$$

where $\bar{\mathbf{u}}_D$ is the average surface velocity ("seepage" or Darcy velocity). Equation (1) represents the macroscopic continuity equation for an incompressible fluid.

Macroscopic Momentum Equation

where $-\rho\phi\overline{\langle \mathbf{u}'\mathbf{u}' \rangle}^{i}$ is the macroscopic Reynolds stress and

$$\left[\nabla \cdot \left(\rho \frac{\bar{\mathbf{u}}_D \bar{\mathbf{u}}_D}{\phi}\right)\right] = -\nabla(\phi \langle \bar{p} \rangle^{i}) + \mu \nabla^2 \bar{\mathbf{u}}_D + \nabla \cdot (-\rho\phi \overline{\langle \mathbf{u}'\mathbf{u}' \rangle}^{i}) - \left[\frac{\mu\phi}{K}\bar{\mathbf{u}}_D + \frac{c_F \phi \rho |\bar{\mathbf{u}}_D| \bar{\mathbf{u}}_D}{\sqrt{K}}\right] \tag{2}$$

the last two terms represent the Darcy–Forchheimer contributions. Further, the symbol K is the porous medium permeability, c_F is the form drag coefficient (Forchheimer coefficient), $\langle \bar{p} \rangle^{i}$ is the intrinsic average pressure of the fluid, ρ is the fluid density, μ represents the fluid viscosity, and ϕ is the porosity. Here, it is also important to acknowledge a possible influence of the medium morphology on macroscopic models that, in principle, do not explicitly account for any effect of turbulence such as the inclusion of the macroscopic Reynolds Stress tensor of Eq. (2). In fact, recent literature results by Bhattacharya et. al. (2002) propose correlations for the inertia coefficient c_F as a function of medium and flow properties. In the path here followed, however, one unique value for the inertia coefficient will be used when presenting macroscopic results later. Here, the explicit accounting for turbulent transport, while keeping a unique macroscopic inertia coefficient, can be seen as an alternative path on adjusting the Forchheimer coefficient for large values of Re. A model for the macroscopic Reynolds Stresses $-\rho\phi\overline{\langle \mathbf{u}'\mathbf{u}' \rangle}^{i}$, required in the present formulation, is given below.

Macroscopic Reynolds Stress

A macroscopic linear stress–strain rate relationship was given by Pedras and de Lemos (2001a) as

$$-\rho\phi\overline{\langle \mathbf{u}'\mathbf{u}' \rangle}^{i} = \mu_{t_\phi} \langle \bar{\mathbf{D}} \rangle^{v} - \frac{2}{3}\phi\rho\langle k \rangle^{i}\mathbf{I} \tag{3}$$

in analogy with clear flow cases. In Eq. (3) the term

$$\langle \overline{\mathbf{D}} \rangle^{v} = \left[\nabla \overline{\mathbf{u}}_D + [\nabla \overline{\mathbf{u}}_D]^T \right] \tag{4}$$

represents the mean deformation tensor and **I** is the unity tensor.

Macroscopic Eddy Viscosity

$$\mu_{t\phi} = \rho c_\mu \frac{\langle k \rangle^{i2}}{\langle \varepsilon \rangle^{i}} \tag{5}$$

where $c_\mu = 0.09$ and $\langle k \rangle^{i}$ and $\langle \varepsilon \rangle^{i}$ are the intrinsic averages of the turbulent kinetic energy and its dissipation rate, respectively.

Macroscopic Turbulent Kinetic Energy Equation

$$\rho \nabla \cdot (\overline{\mathbf{u}}_D \langle k \rangle^{i}) = \nabla \cdot \left[(\mu + \frac{\mu_{t_\phi}}{\sigma_k}) \nabla (\phi \langle k \rangle^{i}) \right]$$
$$-\rho \langle \overline{\mathbf{u}'\mathbf{u}'} \rangle^{i} : \nabla \overline{\mathbf{u}}_D + c_k \rho \frac{\phi \langle k \rangle^{i} |\overline{\mathbf{u}}_D|}{\sqrt{K}} - \rho \phi \langle \varepsilon \rangle^{i} \tag{6}$$

where $-\rho\phi \langle \overline{\mathbf{u}'\mathbf{u}'} \rangle^{i}$ is defined by Eq. (3) and $\sigma_k = 1.0$.

Macroscopic Dissipation Rate of Turbulent Kinetic Energy Equation

$$\rho \nabla \cdot (\overline{\mathbf{u}}_D \langle \varepsilon \rangle^{i})$$
$$= \nabla \cdot \left[(\mu + \frac{\mu_{t_\phi}}{\sigma_\varepsilon}) \nabla (\phi \langle \varepsilon \rangle^{i}) \right] + c_{1\varepsilon} (-\rho \langle \overline{\mathbf{u}'\mathbf{u}'} \rangle^{i} : \nabla \overline{\mathbf{u}}_D) \frac{\langle \varepsilon \rangle^{i}}{\langle k \rangle^{i}}$$
$$+ c_{2\varepsilon} c_k \rho \frac{\phi \varepsilon_\phi |\overline{\mathbf{u}}_D|}{\sqrt{K}} - c_{2\varepsilon} \rho \phi \frac{\langle \varepsilon \rangle^{i2}}{\langle k \rangle^{i}} \tag{7}$$

where $\sigma_\varepsilon = 1.33$, $c_{1\varepsilon} = 1.44$, $c_{2\varepsilon} = 1.92$, and c_k assumes a value equal to 0.28 found by Pedras and de Lemos (2001a–c, 2003).

It is worthwhile to mention that the surface volume average quantities are related to the intrinsic average quantities through the porosity ϕ as

$$\langle \varphi \rangle^{v} = \phi \langle \varphi \rangle^{i} \tag{8}$$

Also, the equations given above are valid for the clear medium as well, setting $\phi = 1$ ($K \to \infty$) and discarding the last two terms in Eq. (2).

Macroscopic Nonlinear Model

In this work, results produced by NLEVMs are investigated. Differently from the linear stress–strain rate relationship Eq. (3), a more general nonlinear constitutive equation will be employed. These models originated in a general proposal done by Pope (1975). However, in the 1980s such closures had greater progress, particularly due to the works of Speziale (1987), Nisizima and Yoshizawa (1987), Rubinstein and Barton (1990), and Shih et. al. (1993) among others. In these works, quadratic products were introduced involving the strain rate and vorticity tensors with different derivations and calibrations for each model. These quadratic forms produce a certain anisotropy degree among the normal stresses, which make it possible to predict, among other processes, the presence of secondary motion in noncircular ducts.

The macroscopic nonlinear turbulence model here proposed is constituted by the same system of Eqs. (1)–(7) formerly given by Pedras and de Lemos (2001a). The sole difference between both macroscopic models (linear and nonlinear) lies in the expression for the macroscopic Reynolds Stress. Using indexed notation for clarity and keeping terms to the second order, this new macroscopic nonlinear stress-strain rate equation can be rewritten in the form

$$-\rho\phi \langle \overline{u_i' u_j'} \rangle^{i} = \left(\mu_{t_\phi} \langle \overline{D}_{ij} \rangle^{v} \right)^{L}$$
$$-\left(c_{1NL}\, \mu_{t_\phi} \frac{\langle k \rangle^{i}}{\langle \varepsilon \rangle^{i}} \left[\langle \overline{D}_{ik} \rangle^{v} \langle \overline{D}_{kj} \rangle^{v} - \frac{1}{3} \langle \overline{D}_{kl} \rangle^{v} \langle \overline{D}_{kl} \rangle^{v} \delta_{ij} \right] \right)^{NL1}$$
$$-\left(c_{2NL}\, \mu_{t_\phi} \frac{\langle k \rangle^{i}}{\langle \varepsilon \rangle^{i}} \left[\langle \overline{\Omega}_{ik} \rangle^{v} \langle \overline{S}_{kj} \rangle^{v} + \langle \overline{\Omega}_{jk} \rangle^{v} \langle \overline{S}_{ki} \rangle^{v} \right] \right)^{NL2}$$
$$-\left(c_{3NL}\, \mu_{t_\phi} \frac{\langle k \rangle^{i}}{\langle \varepsilon \rangle^{i}} \left[\langle \overline{\Omega}_{ik} \rangle^{v} \langle \overline{\Omega}_{jk} \rangle^{v} - \frac{1}{3} \langle \overline{\Omega}_{lk} \rangle^{v} \langle \overline{\Omega}_{lk} \rangle^{v} \delta_{ij} \right] \right)^{NL3}$$
$$-\frac{2}{3} \phi \delta_{ij} \rho \langle k \rangle^{i} \tag{9}$$

where δ_{ij} is the Kronecker delta; the superscripts *L* and *NL* indicate linear and nonlinear contributions; $\mu_{t\phi}$ is again the macroscopic turbulent viscosity given by Eq. (5); and $\langle \overline{D}_{ij} \rangle^{v}$ and $\langle \overline{\Omega}_{ij} \rangle^{v}$ are the deformation and vorticity tensors, written in the indexed form, respectively, as

$$\langle \overline{D}_{ij} \rangle^{v} = \left(\frac{\partial \overline{u}_{D_i}}{\partial x_j} + \frac{\partial \overline{u}_{D_j}}{\partial x_j} \right),$$
$$\langle \overline{\Omega}_{ij} \rangle^{v} = \left(\frac{\partial \overline{u}_{D_i}}{\partial x_j} + \frac{\partial \overline{u}_{D_j}}{\partial x_i} \right) \tag{10}$$

Table 1 shows the different values of c_μ, c_{1NL}, c_{2NL}, and c_{3NL} proposed in the literature. Note that Eq. (3) is recovered if constants c_{1NL}, c_{2NL}, and c_{3NL} in Eq. (9) are set to zero.

Table 1

Nonlinear turbulence models

Models	c_μ	c_{1NL}	c_{2NL}	c_{3NL}	Extra terms
Nisizima and Yoshizawa (1987)	0.09	–0.76	0.18	1.04	
Speziale (1987)	0.09	–0.1512	0.0	0.0	T_{SPE}
Rubinstein and Barton (1990)	0.0845	0.68	0.14	–0.56	
Shin et al. (1993)	$\dfrac{2/3}{1.25 + s + 0.9\Omega}$	$\dfrac{0.75}{c_\mu\,(1000 + s^3)}$	$\dfrac{3.8}{c_\mu\,(1000 + s^3)}$	$\dfrac{4.8}{c_\mu\,(1000 + s^3)}$	
Park and Sung (1995)	0.09	0.6	0.4	0.005	

$$T_{SPE} = -0.3024\mu_{t_\phi}\frac{\langle k\rangle^i}{\langle\varepsilon\rangle^i}\left\{\tilde{D}_{ij} - \tfrac{1}{3}\tilde{D}_{mm}\delta_{ij}\right\}, \quad \text{where} \quad \tilde{D}_{ij} = \frac{\partial\langle\bar{D}_{ij}\rangle^v}{\partial t} + \vec{V}_D\cdot\langle\bar{D}_{ij}\rangle^v - \frac{\partial V_{i_D}}{\partial x_k}\langle\bar{D}_{kj}\rangle^v - \frac{\partial V_{j_D}}{\partial x_k}\langle\bar{D}_{ki}\rangle^v$$

$$\text{and} \quad s = \frac{\langle k\rangle^i}{\langle\varepsilon\rangle^i}\sqrt{\tfrac{1}{2}\langle\bar{D}_{ij}\rangle^v\langle\bar{D}_{ij}\rangle^v}, \quad \Omega = \frac{\langle k\rangle^i}{\langle\varepsilon\rangle^i}\sqrt{\tfrac{1}{2}\langle\bar{\Omega}_{ij}\rangle^v\langle\bar{\Omega}_{ij}\rangle^v}$$

It is important to emphasize here that values in Table 1 were obtained in the literature for models developed for a clear medium, although Eq. (2) will be applied to both porous and clear domains. Here, in the absence of better information, no modifications are introduced in the constants or model parameters when Eq. (2) is used within the porous structure.

Interface Conditions

The interface between the porous medium and the clear fluid is treated as follows (Ochoa Tapia and Whitaker, 1995) and the interface conditions can be expressed as

$$\bar{\mathbf{u}}_{D,\text{clear medium}} = \bar{\mathbf{u}}_{D,\text{porous medium}} \tag{11}$$

$$\langle\bar{p}\rangle^i_{\text{clear medium}} = \langle\bar{p}\rangle^i_{\text{porous medium}} \tag{12}$$

$$\frac{1}{\phi}\frac{\partial U_{D\|,\text{porous med.}}}{\partial n} - \frac{\partial U_{D\|,\text{clear med.}}}{\partial n} = \frac{\beta}{\sqrt{K}}U_{D\|,\text{porous med.}} \tag{13}$$

where $U_{D\|}$ is the component of the average surface velocity parallel to the interface, n is the coordinate normal to the interface from the porous medium to the clear medium, and β is a coefficient that expresses the stress jump condition at the interface. For all of the cases treated in this article, the coefficient β was assumed to be null, i.e., $\beta = 0$. The effect of using a different value of such coefficient is shown below.

NUMERICAL METHOD

Flow over the backward-facing-step of Fig. 1, with and without the porous insert, was computed using the control-volume method applied to a boundary-fitted coordinate system. The SIMPLE algorithm was used to relax the algebraic equations. Classical wall function was employed to describe the flow near the wall. Results were obtained considering an inlet Reynolds number of Re = 132,000 based on the height of the step H, which in this work was taken as equal to 0.1 m. Inlet conditions for U, k, and ε were used according to values proposed by Heyerichs and Pollard (1996). All boundary condition values are illustrated in Fig. 1. The nonlinear model employed was the closure (Shih et. al., 1993). An orthogonal mesh of size 200×60 was used due to the simplicity of the geometry investigated. In all computations shown below normalized residues, all transport equations involved were brought down to 1×10^{-5}.

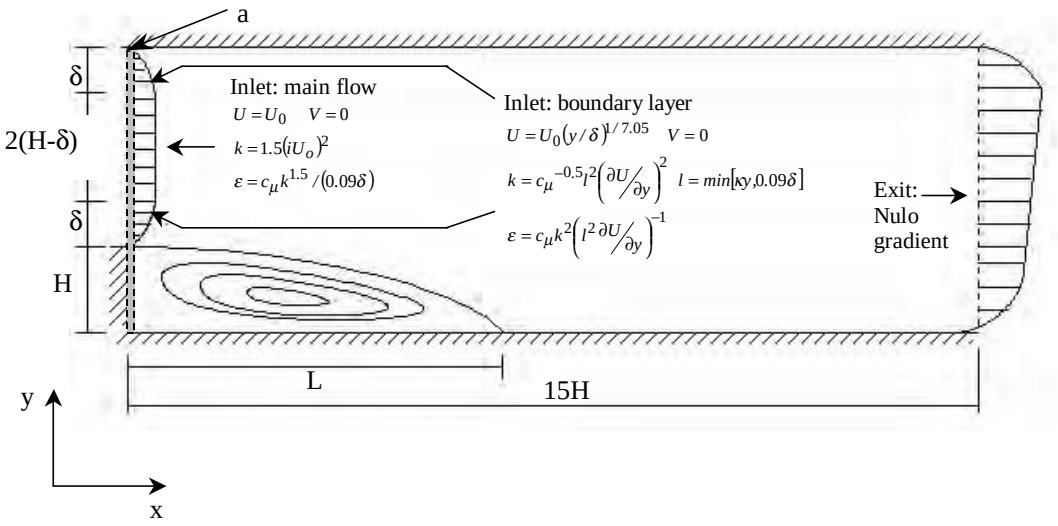

Figure 1. Boundary conditions for turbulent flow past a backward-facing step with porous insert.

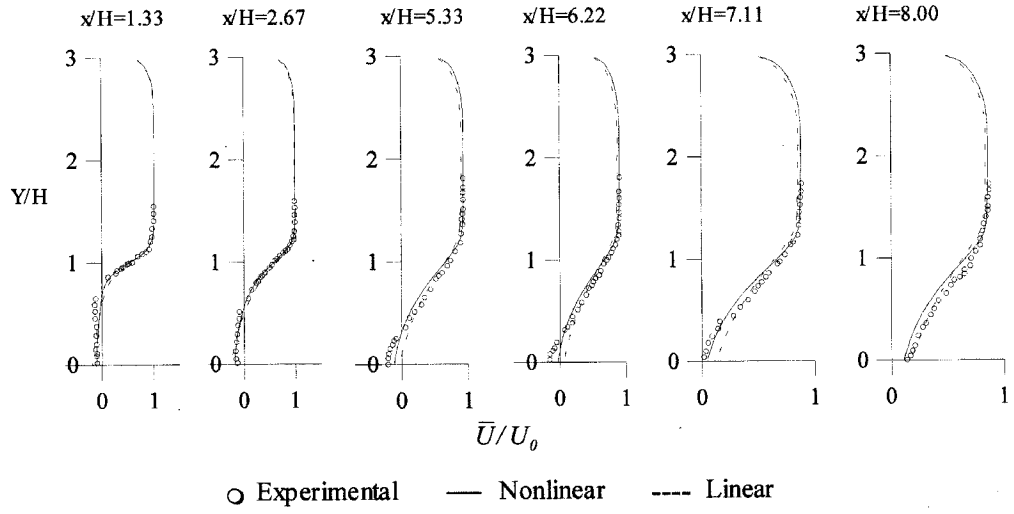

Figure 2. Axial mean velocity profiles along axial coordinate.

RESULTS AND DISCUSSION

Preliminary results for unobstructed flow past a backward-facing-step were obtained in order to assess the performance of the linear and nonlinear turbulence models in clear domains. Numerical parameters for this cases were $a = 0$, $c_F = 0$, $\phi = 1$, and $K \rightarrow \infty$. Figures 2–4 show calculations for the axial velocity, turbulent intensity, and shear stress, respectively, compared with experimental data reported by Kim et. al. (1980). The figures indicate that overall behavior of the mean and statistical flow is reproduced by both linear and nonlinear theories, the latter method being of superior quality when comparing results for the mean and statistical quantities.

Grid independence studies were also conducted with the aim of checking the behavior of the solution as the grid

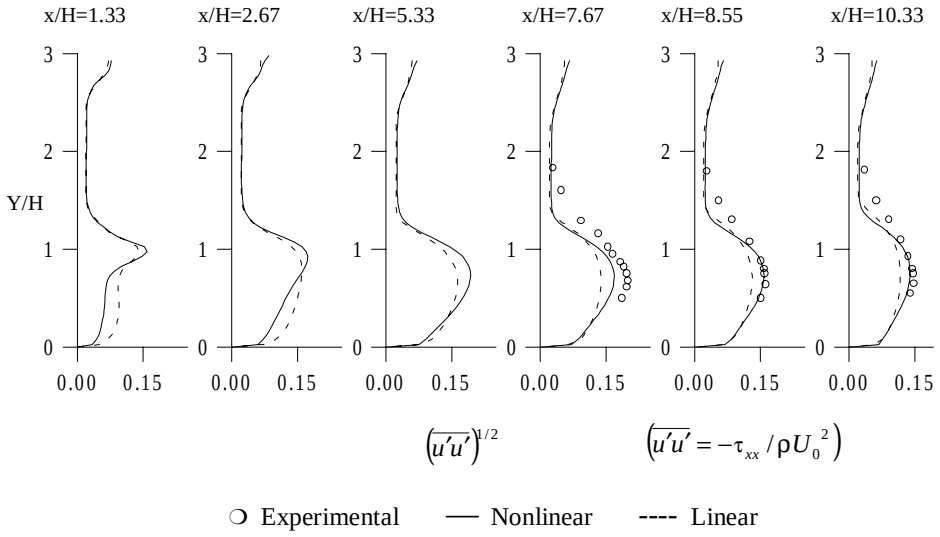

Figure 3. Nondimensional turbulence intensity along axial coordinate compared with experiments by Kim et. al. (1980).

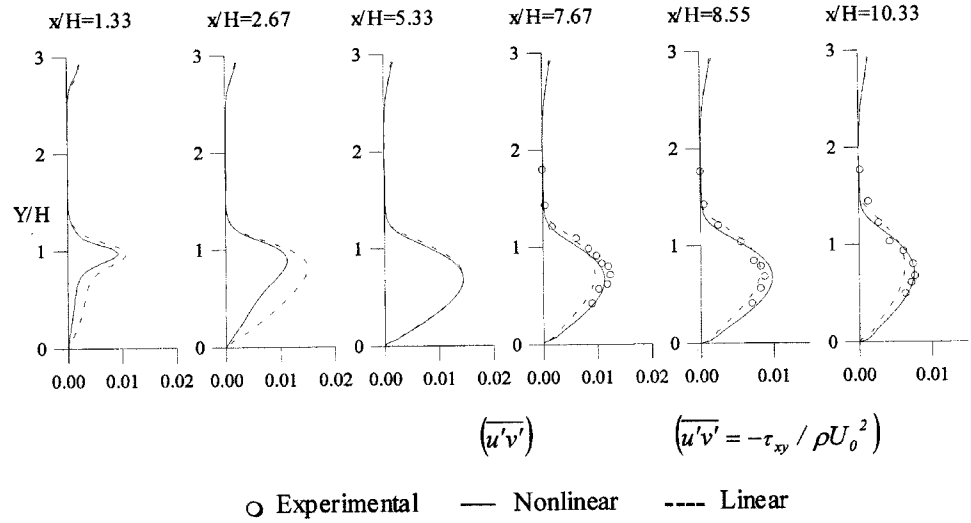

Figure 4. Nondimensional turbulent shear stress compared with experiments by Kim et. al. (1980).

size was varied. Table 2 presents calculations for the reattachment length x_R/H for different grids. One can see that for grids greater than 200 × 60 grid nodes, there is no detectable change in the calculated reattachment length. Based on Table 2, in this work all computations are shown for a mesh of size 200 × 60. With unobstructed results validated, calculations involving the mentioned porous insert can be better accessed.

As such, in the following figures, the effect of coefficient β, channel length L/H, porosity, thickness, and permeability of a porous insert on the flow pattern will be shown for turbulent flow, using both the linear and nonlinear models. In each figure, the streamlines are analyzed without the porous insert and with the porous material for the following thicknesses: $a = 0.15H$, $a = 0.30H$, and $a = 0.45H$, where H is the step height.

Table 2

Separation length as a function of grid size

Model	Dimensions (m)	Grid size	Reattachment length (x_R/H)	Percent deviation from experimental value of $x_R/H = 7.0$
L_HRN	1.5×0.3	150×45	5.50	–21.43
NL_HRN			6.50	–7.14
L_HRN	1.5×0.3	200×60	5.55	–20.71
NL_HRN			6.45	–7.86
L_HRN	1.5×0.3	200×75	5.55	–20.71
NL_HRN			6.45	–7.86
L_HRN	1.8×0.3	240×60	5.55	–20.71
NL_HRN			6.45	–7.86

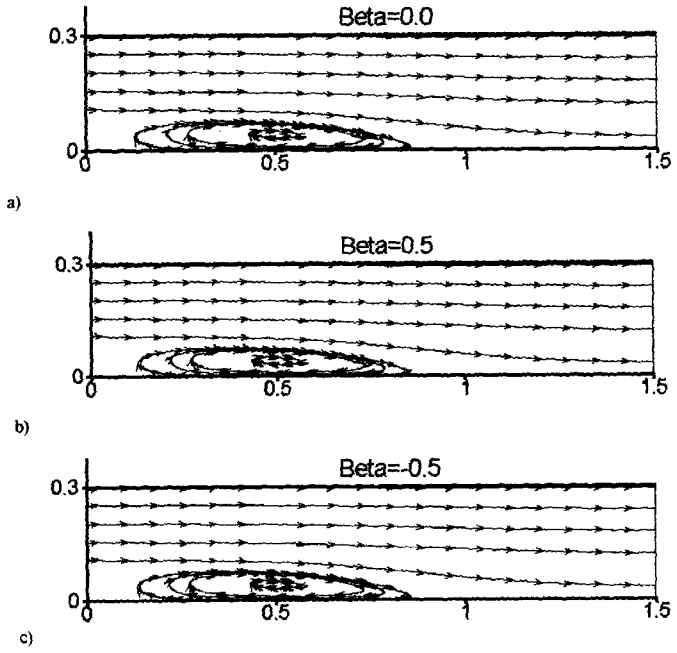

Figure 5. Calculated flow pattern using a linear model with $a = 0.15H$ m, $K = 10^{-6}$ m^2, $\phi = 0.85$: a) $\beta = 0.0$, b) $\beta = 0.5$; c) $\beta = -0.5$.

The effect of using a different coefficient β is shown in Fig. 5. One can see that the flow pattern presents nearly the same behavior regardless of the value used for the jump coefficient in Eq. (13). Further calculations for the friction coefficient along the bottom wall defined as

$$Cf = \frac{\tau_w}{\rho U_0^2/2} \tag{14}$$

are presented in Fig. 6, where a similar behavior can be noted. Since the flow in the geometry of Fig. 1 is mostly *perpendicular* to the interface, the shear stress caused by the fluid at that location is negligible. In fact, previous work on the stress jump condition across an interface for laminar (Silva and de Lemos, 2003a) and turbulent flow (Silva and de Lemos, 2003b**)** *parallel* to a layer of porous material in a channel indicated a substantial modification of the ve-

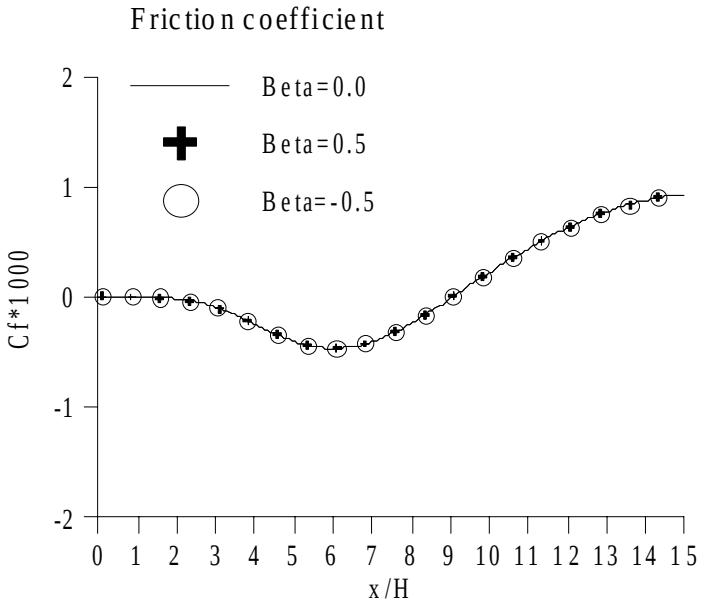

Figure 6. Friction coefficient at bottom surface for β equal to –0.5, 0.0, and 0.5.

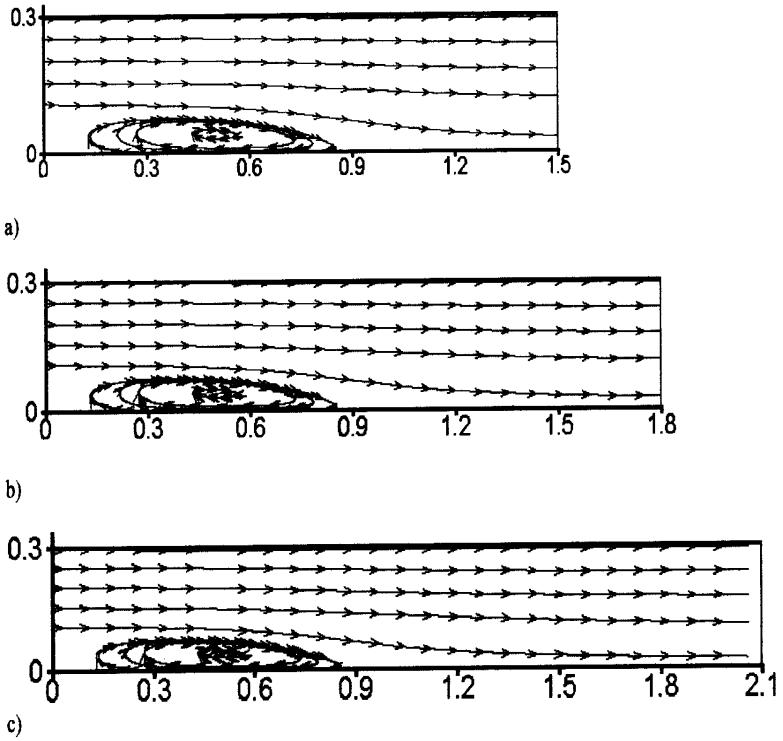

Figure 7. Calculated flow pattern using a linear model with $a = 0.15H$ m, $K = 10^{-6}$ m^2, $\phi = 0.85$: a) $L/H = 15$, grid: 200 × 60, b) $L/H = 18$, grid: 240 × 60; c) $L/H = 21$, grid: 280 × 60.

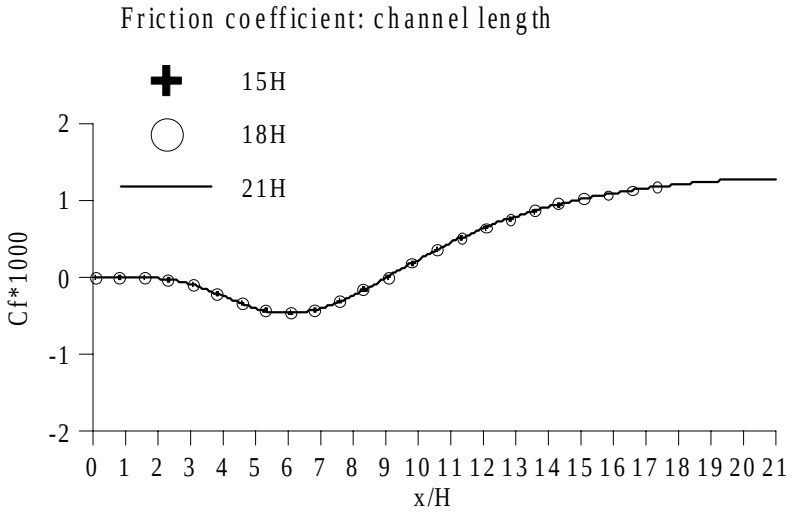

Figure 8. Friction coefficient at bottom surface for different values of *L/H*.

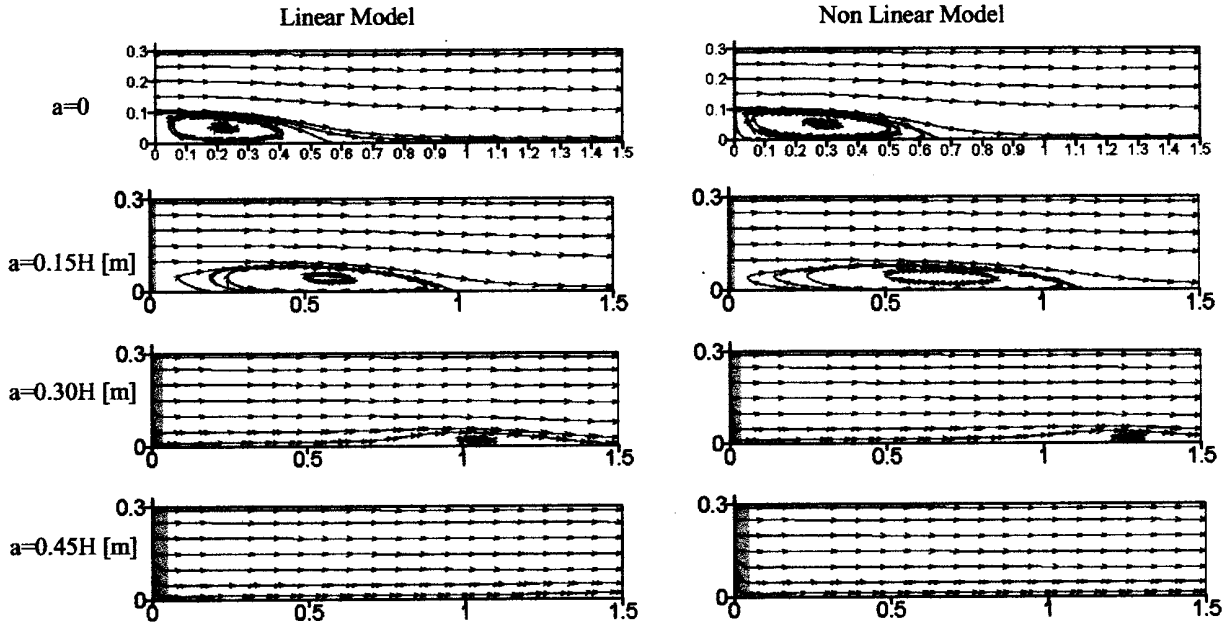

Figure 9. Comparison of streamlines between the linear and nonlinear models for backward-facing-step flow with porous insert, $K = 10^{-6}$ m^2, $\phi = 0.65$.

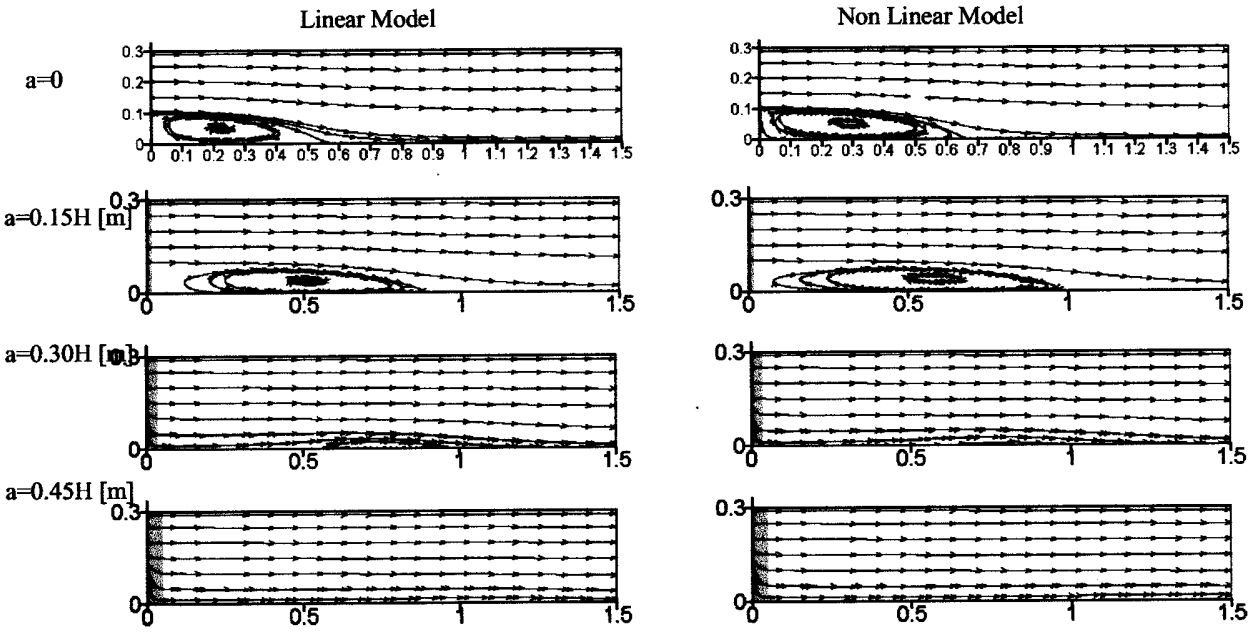

Figure 10. Comparison of streamlines between the linear and nonlinear models for backward-facing-step flow with porous insert, $K = 10^{-6}$ m^2, $\phi = 0.85$.

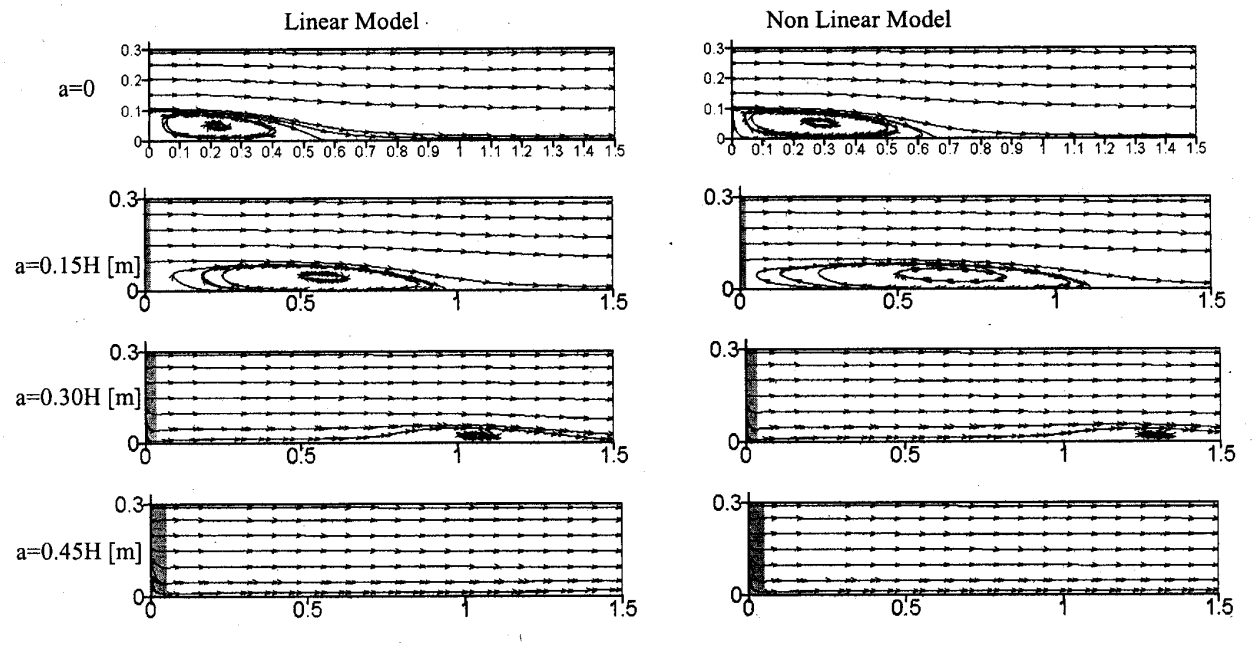

Figure 11. Comparison of streamlines between the linear and nonlinear models for backward-facing-step flow with porous insert, $K = 10^{-7}$ m^2, $\phi = 0.85$.

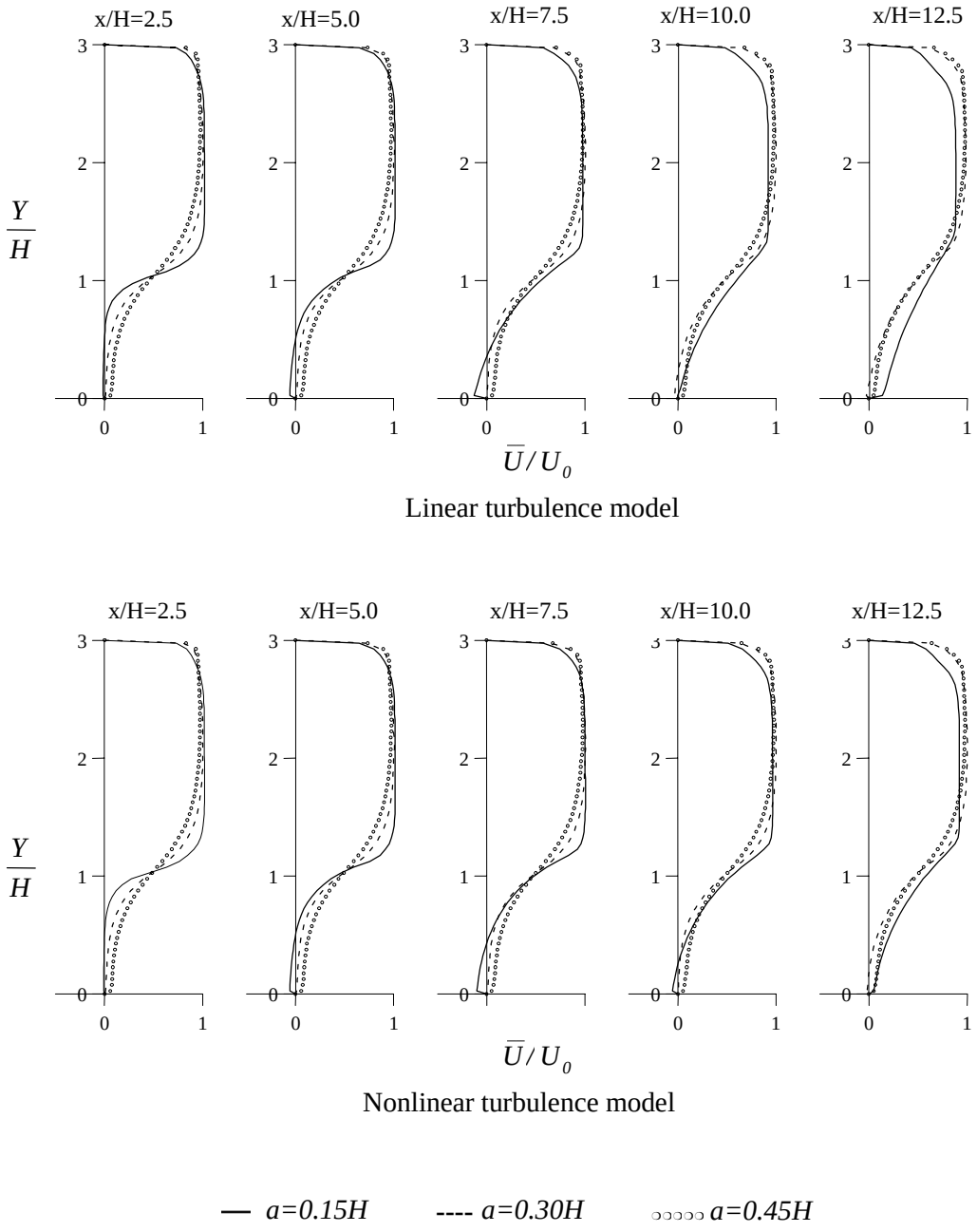

Figure 12. Mean velocity field simulated by linear and nonlinear models. Porous insert with $K = 10^{-6}$ m^2, $\phi = 0.65$.

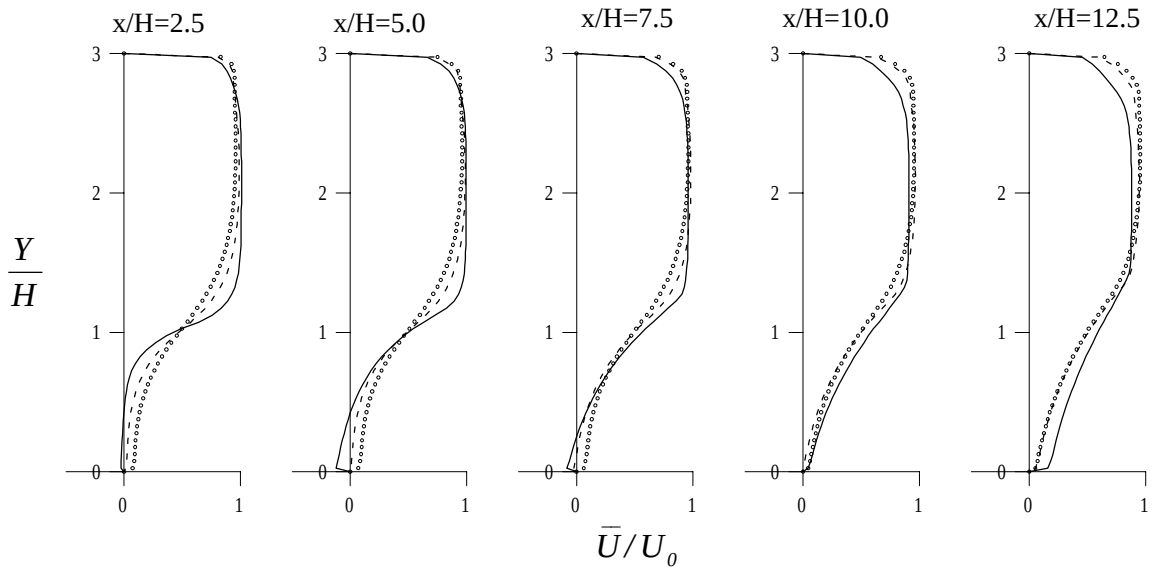

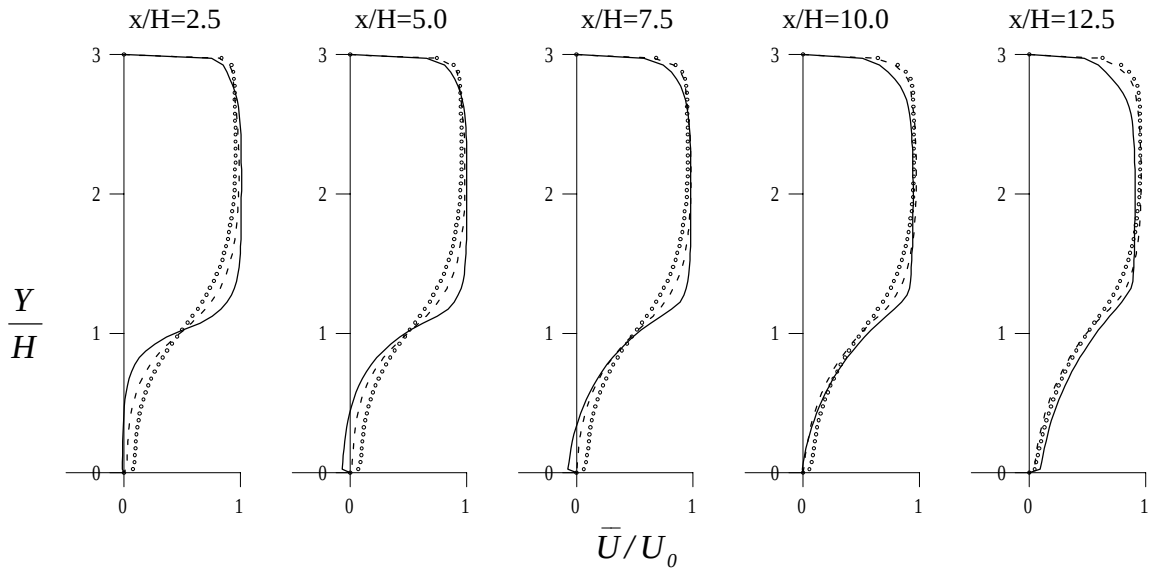

Figure 13. Mean velocity field simulated by linear and nonlinear models. Porous insert $K = 10^{-6}$ m^2, $\phi = 0.85$.

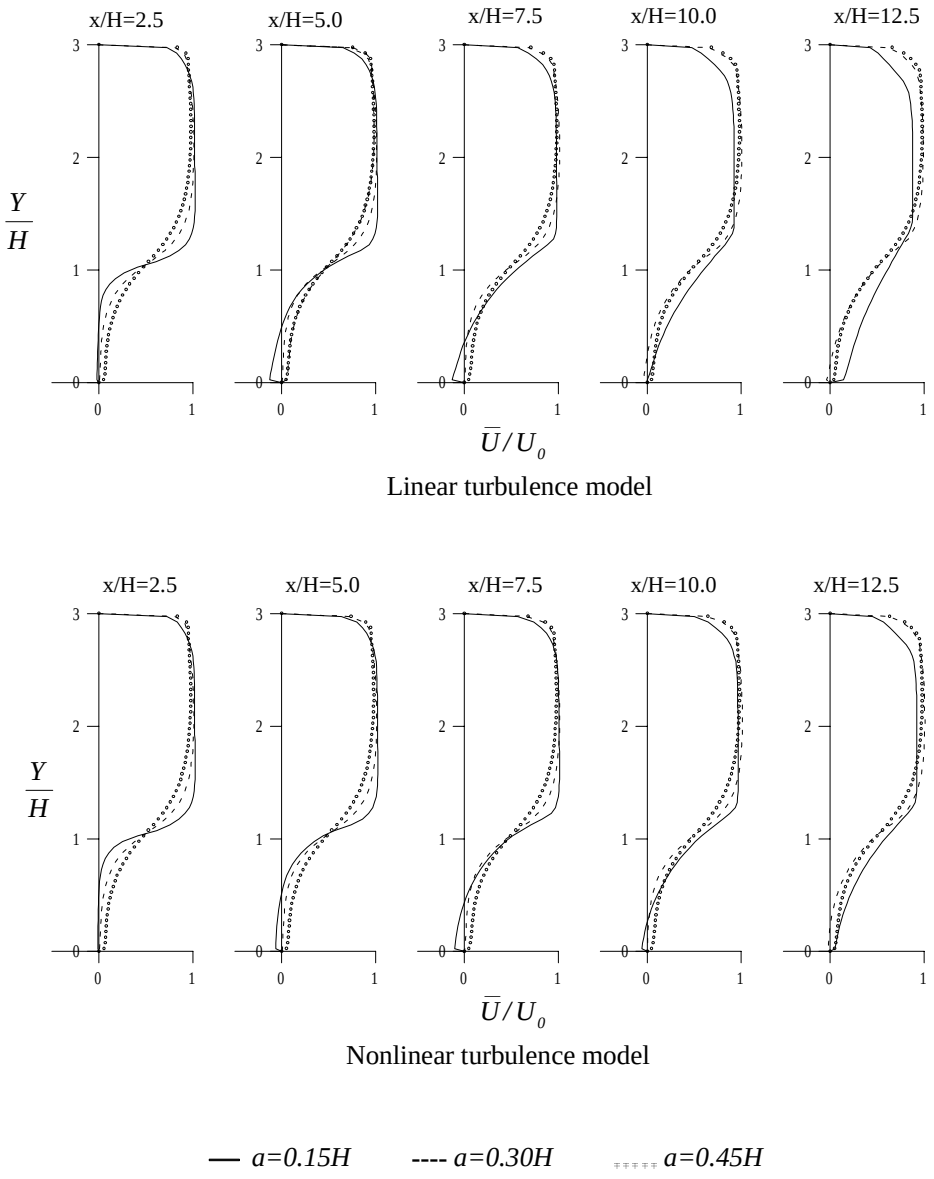

Figure 14. Mean velocity field simulated by linear and nonlinear models. Porous insert with $K = 10^{-7}$ m^2, $\phi = 0.85$.

locity pattern, depending on the mentioned β parameter. Therein, however, the streamlines were aligned to the interface position, corresponding to a different flow configuration than the one explored in the present work.

An indication of the appropriateness of the channel length value used, $L/H = 15$, can be drawn from analyzing Fig. 7 where one can see that the size and shape of the recirculating bubble is nearly the same if the channel is increased. Figure 8 further indicates that no influence is also detected on the friction coefficient, calculated by Eq. (14), if the length of the computational domain is increased. Preliminary results shown so far support the use of 200 × 60 grid nodes, $L/H = 15$, and $\beta = 0$ in all computations to be presented.

Therefore, Figs. 9–11 show comparisons of streamlines between the linear and nonlinear closures considering the following permeability and porosity combinations: Fig. 9) $K = 10^{-6}$ m^2, $\phi = 0.65$; Fig. 10) $K = 10^{-6}$ m^2, $\phi = 0.85$, and

Fig. 11) $K = 10^{-7}$ m^2, $\phi = 0.85$. It can be seen that the size of the recirculation bubble simulated by the linear model, in all cases with porous inserts, is shorter than the one calculated by nonlinear theories. Unfortunately, no experimental data seems to be available in the literature documenting measurements of flow properties in a backward-facing-step with a porous insertion. Also, as the thickness of insert is increased, the recirculation bubble decreases, and for $a = 0.45H$, the recirculation bubble is nearly suppressed, independently of the turbulence model used. A possible explanation for this behavior is that the presence of the porous substrate tends to flatten the Darcy velocity profile due to the two additional flow resistances modelled by the two last terms on the right-hand side of Eq. (2). As such, after a certain developing thickness within the porous matrix, the profile is sufficiently "flat" so that the fluid is "delivered" to the channel with a uniform pressure at each cross-station along the longitudinal x direction.

From the figures, one can further observe that the permeability K and the porosity ϕ of the porous insert also play a role in determining the flow pattern. However, their influence on the flow distribution past the obstacle seems to be not as intense as the effect of the thickness a. Or say, by just increasing the value of a/H one can smooth the flow past the expansion, damping any existing recirculating stream.

Finally, Figs. 12–14 show the mean velocity field $\overline{U}/U_0$ at some stations along the channel with the porous insert. It can be noted that the deviations between the results produced with linear and nonlinear theory decrease as the thickness of insert increases. Further, for $a = 0.45H$, both models produce nearly the same results.

CONCLUSIONS

In this work, two turbulence models (linear and nonlinear), using wall functions, have been used to simulate turbulent flow past a backward-facing step with a porous insert. Parameters such as porosity ϕ, permeability K, and thickness a of the porous material were varied in order to analyze their effects on the flow pattern.

For validation, results without the insert were compared with experimental data of Kim et al. (1980). The experimental value for the separation length given in the literature is $x_R/H = 7.0$. The linear and nonlinear models resulted in $x_R/H = 5.55$ and $x_R/H = 6.45$, respectively, indicating an advantage of nonlinear closures in predicting more realistic results.

Figures 9–11 showed that the recirculating bubble simulated with the linear model was always shorter than the one calculated with nonlinear theories. Also, results indicate that the thickness of the insert had a more pronounced effect in suppressing the recirculation bubble than other parameters, such as the permeability or the porosity. It has also been observed that the total damping of the recirculation bubble occurred for $a = 0.45H$, independently of the turbulence model employed.

In summary, the following conclusions can then be drawn from this work:

1. The developed code and numerical methodology used are in agreement with findings in the literature as far as simulating unobstructed suddenly expanding flows in channels.

2. For the configuration in question, which includes a porous insert of thickness a at the sudden expansion, the recirculating bubble calculated with linear models gave shorter reattachment lengths than those simulated via a nonlinear stress-strain rate relationship.

3. For the cases analyzed here, the thicker the insert, the lower the differences in the value of x_R calculated with the two models. This behavior might be explained by the fact that inside the porous material additional forces exerted by the solid on the fluid tend to flatten the Darcy velocity profiles. As such, as the porous matrix gets thicker, recirculating bubbles tend to disappear regardless of the turbulence model used.

ACKNOWLEDGMENTS

The authors would like to thank FAPESP and CNPq, Brazil, for their financial support during the preparation of this work.

REFERENCES

Assato, M. and de Lemos, M. J. S., Numerical treatment and applications of a nonlinear eddy viscosity model for high and low Reynolds formulations (in Portuguese), *Proceedings of the 2nd ETT—Brazilian School on Transition and Turbulence*, Uberlandia, MG, Brazil, Dec. 11–15, Brazilian Association of Mechanical Sciences, Rio de Janeiro, pp. 459–483, 2000.

Assato, M. and de Lemos, M. J. S., Numerical simulation of turbulent flow through axisymmetric stenosis using linear and nonlinear eddy-viscosity models, *Proceedings of the 16th COBEM–Braz. Cong. Mech. Eng*, Uberlandia, MG, Brazil, Brazilian Association of Mechanical Sciences, Rio de Janeiro, (on CD-Rom), 2001.

Beavers, G.. S. and Joseph, D. D., Boundary conditions at a naturally permeable wall, *J. Fluid Mech*., vol. 30, pp. 197–207, 1967.

Braga, E. J. and de Lemos, M. J. S., Turbulent natural cnvection in a porous square cavity computed with a macroscopic *k*-ε model, *Int. J. Heat Mass Transfer*, vol. 47, no. 26, pp. 5635–5646, 2004.

Brinkman, H. C., Calculations of the flow of heterogeneous mixture through porous media, *Appl. Sci. Res*., vol. 2, pp. 81–86, 1948.

Chan, E. C., Lien, F. S., and Yovanovich, M. M., Macroscopic numerical study of forced convective heat transfer in a back-step channel through porous layer, *Proceedings of NTHC2000—ASME National Heat Transfer Conf*., Aug. 20–22, Pittsburgh, ASME, New York, (jn CD-Rom), 2000.

de Lemos, M. J. S., Anisotropic turbulent transport modeling for rod-bundle, *Int. J. Heat Technol*., vol. 6, no. 1–2, pp. 27-37, 1988.

de Lemos, M. J. S. and Braga. E. J., Modeling of turbulent natural convection in saturated rigid porous media, *Int. Commun. Heat Mass Transfer*, vol. 30, no. 30, pp. 615–624, 2003.

de Lemos, M. J. S.. and Mesquita, M. S., Turbulent mass transport in saturated rigid porous media, *Int. Commun. Heat Mass Transfer*, vol. 30, no. 1. pp. 105–113, 2003.

de Lemos, M. J. S. and Tofaneli, L. A., Modeling of double-diffusive turbulent natural convection in porous media, *Int. J. Heat Mass Transfer*, vol. 47, no. 19-20, pp. 4221–4231, 2004.

de Lemos, M. J. S. and Sesonske, A., Turbulence modeling in combined convection in liquid-metal pipe flow, *Int. J. Heat Mass Transfer*, vol. 28, no. 6, pp. 1067–1088, 1985.

de Lemos, M. J. S. and Pedras, M. H. J., Recent mathematical models for turbulent flow in saturated rigid porous media, *ASME J. Fluids Eng*., vol. 123, no. 4, pp. 935–940, 2001.

Heyerichs, K. and Pollard, A., Heat transfer in separated and impinging turbulent flows, *Int. J. Heat Mass Transfer*, vol. 39, no. 12, pp. 2385–2400, 1996.

Jones, W. P. and Launder, B. E., The prediction of laminarization with two-equation model of turbulence, *Int. J. Heat Mass Transfer*, vol. 15, pp. 301–314, 1972.

Kim, J., Kline, S. J., and Johnston, J. P., Investigation of a reattaching turbulent shear layer: Flow over a backward-facing step, *ASME J. Fluids Eng*., vol. 102, pp. 302–308, 1980.

Kuznetsov, A. V., Analytical investigation of the fluid flow in the interface region between a porous medium and a clear fluid in channels partially filled with a porous medium, *Int. J. Heat Fluid Flow*, vol. 12, pp. 269–272, 1996.

Kuznetsov, A. V., Influence of the stresses jump condition at the porous-medium/clear-fluid interface on a flow at a porous wall, *Int. Commun. Heat Mass Transfer*, vol. 24, pp. 401–410, 1997.

Kuznetsov, A. V., Fluid mechanics and heat transfer in the interface region between a porous medium and a fluid layer: A boundary layer solution, *J. Porous Media*, vol. 2, no 3, pp. 309–321, 1999.

Lage, J. L., de Lemos, M. J. S., and Nield, D. A., Modeling turbulence in porous media, *Transport Phenomena in Porous Media*, Kidlington, UK, Ingham, D. B. and Pop, I. (eds.),Vol. 2, pp. 198–230, 2002.

Lumley, J. L., Toward a turbulent constitutive relation, *J. Fluid Mech*., vol. 41, pp. 413–434, 1970.

Nield, D. A. and Bejan, A., *Convection in Porous Media*, 2nd ed., Springer, New York, 1999.

Nisizima, S. and Yoshizawa, A., Turbulent channel and Couette flows using an anisotropic *k*–ε-model, *AIAA J*., vol. 25, no. 3, pp. 414–420, 1987.

Ochoa-Tapia, J. A. and Whitaker, S., Momentum transfer at the boundary between a porous medium and a homogeneous fluid—I. Theoretical development, *Int. J. Heat Mass Transfer*, vol. 38, pp. 2635–2646, 1995.

Park, T. S. and Sung, H. J., A nonlinear low-Reynolds-number k-epsilon model for turbulent separated and reattaching flows, *Int. J. Heat Mass Transfer*, vol. 8, pp. 2657–2666, 1995

Pedras, M. H. J. and de Lemos, M. J. S., On the definition of turbulent kinetic energy for flow in porous media, *Int. Commun. Heat Mass Transfer*, vol. 27, no 2, pp. 211–220, 2000.

Pedras, M. H. J. and de Lemos, M. J. S., Macroscopic turbulence modeling for incompressible flow through undeformable porous media, *Int. J. Heat Mass Transfer*, vol. 44, no. 6, pp. 1081–1093, 2001a.

Pedras, M. H. J. and de Lemos, M. J. S., Simulation of turbulent flow in porous media using a spatially periodic array and a low Re two-equation closure, *Numer. Heat Transfer*, Part A, vol. 39, no. 1, pp. 35–59, 2001b.

Pedras, M. H. J. and de Lemos, M. J. S., On mathematical description and simulation of turbulent flow in a porous medium formed by an array of elliptic rods, *ASME J. Fluids Eng*., vol. 123, no. 4, pp. 941–947, 2001c.

Pedras, M. H. J. and de Lemos, M. J. S., Computation of turbulent flow in porous media using a low Reynolds *k*–ε-model and an infinite array of transversally-displaced elliptic rods, *Numer. Heat Transfer*, Part A, vol. 43, no. 6, pp. 585–602, 2003.

Pope, S. B., A more general effective-viscosity hypothesis, *J. Fluid Mech*., vol. 72, pp. 331–340, 1975.

Rivlin, R. S., The relation between the flow of non-Newtonian fluids and turbulent Newtonian fluids, *Q. Appl. Math*., vol. 15, pp. 212–215, 1957.

Rocamora, Jr., F. D. and de Lemos, M. J. S., Analysis of convective heat transfer for turbulent flow in saturated porous media, *Int. Commun. Heat Mass Transfer*, vol. 27, no. 6, pp. 825–834, 2000a.

Rocamora, Jr., F. D. and de Lemos, M. J. S., Heat transfer in suddenly expanded flow in a channel with porous inserts, Proc. of IMECE02–ASME, Int. Mech. Eng. Congr. & Expo., Oriando, Flórida, Nov. 5–10, vol. HTD-366, no. 5, ASME, New York, pp. 191–196, 2000c.

Rodi, W., The Prediction of Free Turbulent Boundary Layers by Use of a Two-Equation Model of Turbulence, PhD Thesis, University of London, 1972.

Rubinstein, R. and Barton, J. M., Renormalization group analysis of the stress transport equation, *Phys. Fluids A*, vol. 2, no. 8, pp. 1472–1476, 1990.

Shih, T. H., Zhu, J., and Lumley, J. L., A Realizable Reynolds Stress Algebraic Equation Model, NASA TM-105993, 1993.

Silva, R. A. and de Lemos, M. J. S., Numerical analysis of the stress jump interface condition for laminar flow over a porous layer, *Numer. Heat Transfer*, Part A, Vol. 43, no. 6, pp. 603–617, 2003a.

Silva, R. A. and de Lemos, M. J. S., Turbulent flow in a channel occupied by a porous layer considering the stress jump at the interface, *Int. J. Heat Mass Transfer*, vol. 46, no. 26, pp. 5113–5121, 2003b.

Speziale, C. G., On nonlinear *k–l* and *k–*ε-models of turbulence, *J. Fluid Mech.*, vol. 176, pp. 459–475, 1987.

Vafai, K. and Kim, S. J., Fluid mechanics of the interface region between a porous medium and a fluid layer: An exact solution, *Int. J. Heat Fluid Flow*, vol. 11, pp. 254–256, 1990.

Vafai, K. and Tien, C. L., Boundary and inertia effects on flow and heat transfer in porous media, *Int. J. Heat Mass Transfer*, vol. 24, pp. 195–203, 1981.